Site-specific x-ray absorption spectroscopy of electron traps by x-ray-induced displacement current measurement

Masashi Ishii*

Japan Synchrotron Radiation Research Institute (JASRI), SPring-8, Mikaduki, Sayo-gun, Hyogo 679-5198, Japan

(Received 8 March 2001; revised manuscript received 7 August 2001; published 4 February 2002)

The concept of ‘‘x-ray-induced displacement currents’’ is introduced for x-ray absorption spectroscopy (XAS) in the local structure analysis of electron traps. Since such a displacement current (orthogonal to the conduction current, i.e., the conventional photocurrent) is responsive to localized electrons, it allows XAS to provide site-specific x-ray absorption of electron traps. Capacitance x-ray absorption fine structure (Capacitance XAFS) measurement based on this idea is adopted for defect observation in a compound semiconductor, and the result is a nonlinear dependence of the XAFS signal intensity on the bias voltage applied to the sample. This nonlinearity is formulated by the theory of the Schottky barrier diode, which is used for the capacitor formation; the x-ray-induced photoionization of the defect reduces the trapping charge at interface between depletion layer and semiconductor, resulting in capacitance increase. The temperature dependence of capacitance XAFS spectra indicates that the conduction current has no site specificity owing to the mixing of the photocarrier from the defect and crystal sites, while the x-ray-induced displacement current provides site-specific spectra independent of the conduction current.

DOI: 10.1103/PhysRevB.65.085310 PACS number(s): 78.70.Dm, 61.72.Ff, 61.10.Ht, 71.55.Eq

I. INTRODUCTION

In recent years, the brilliant x rays from a synchrotron radiation (SR) light source have been extensively applied to material science by using a variety of experimental techniques, such as x-ray diffraction,[1] x-ray scattering,[2] and x-ray absorption.[3] It is well known that x-ray absorption spectroscopy (XAS) has fine structures in its spectra around the absorption edge, i.e., x-ray absorption fine structures (XAFS).[4] These structures near the absorption edge probe the electronic state owing to the resonant inner-shell absorptions, and the Fourier transformations of the XAFS over the wide energy range provide structural information, such as the bond length and the coordination number around a specific atom selected by the absorption edge energy.[5,6] Because of this atom selectivity, hard x rays with photon energies of $\sim$10 keV can be used for the local structure analysis of interspersed atoms in solids[7] and liquids.[8]

On the other hand, analytical objects have become diversified by the progress in material science. The fine control of the valence energy level with an accuracy of $\sim$meV has been demanded in the design of advanced electric and optical devices.[9,10] In fact, in recent material fabrication techniques, precise atom manipulation has resulted in well-defined heterogeneous systems, such as quantum structures.[11] Not only material selection but also structural modification at the atomic level has become crucial. Under such circumstances, the atom selectivity in the conventional XAFS analysis is insufficient for material evaluation purposes; site specificity is necessary for local structure analysis of a heterogeneous system. However, the x-ray photon energy of $\sim$10 keV used in XAS is too large to identify energy differences of the order of $\sim$meV at valence states caused by structural modifications.[12] Moreover, the Fourier transformation of an XAFS spectrum merely provides average information about a heterogeneous system.

Various trials for the achievement of site-specific XAFS measurement have already been demonstrated.[13–17] For instance, x-ray-excited optical luminescence (XEOL) successfully offers site-specific XAFS spectra of optically active centers with its x-ray photon energy dependence (XEOL-XAFS).[18,19] This technique selectively evaluates the keV photon absorption of the optical centers by the meV optical emission. The success of XEOL-XAFS suggests that the detection of valence phenomena induced by inner-shell excitation is essential for the site specificity of the XAFS measurement. Recently, a capacitance XAFS method was proposed in which capacitance changes are used to evaluate the inner-shell absorption.[16,20] In this method, a particular valence state modified by x rays is electrically detected for the site specificity. The previous paper discussed the site specificity to defects involved in this method. However, no clarification was provided on the details of x-ray-induced valence modification.

In this paper, the idea of ‘‘x-ray-induced displacement currents’’ is introduced. This electromagnetic idea provides an essence of the site specificity in the capacitance XAFS measurement. The origin of the polarized charge for the displacement currents is also discussed. The properties of absorption signals of capacitance XAFS under various experimental conditions are formalized based on these macro and microscopic schemes.

II. SITE-SPECIFIC XAFS MEASUREMENT USING DISPLACEMENT CURRENT

In the conventional XAFS method, photoelectrons are detected by the schematic shown in Fig. 1(a), because a photocurrent caused by a photoelectron is proportional to the value of x-ray absorption coefficient μ.[21,22] A high voltage power supply E_{DC}, and an electrode opposite to the sample, are normally used for the collection of a photoelectron from a sample. Figure 1(a′) gives an equivalent circuit of this

 ©2002 The American Physical Society

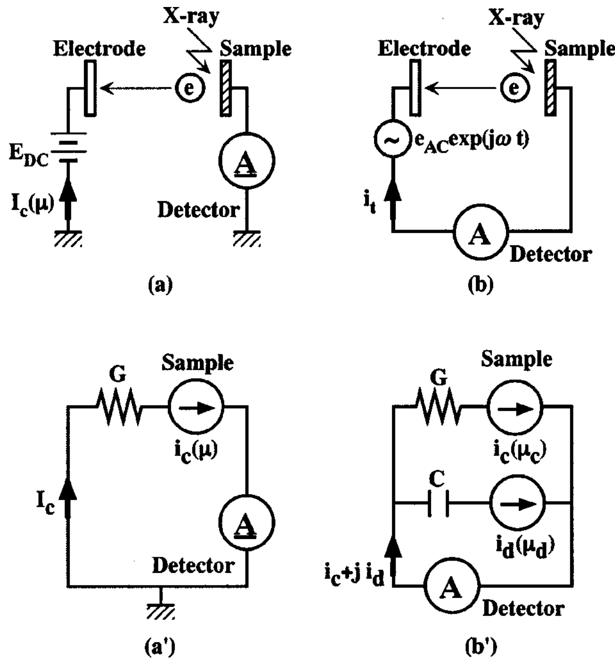

FIG. 1. (a) Schematic setup for the conventional XAFS measurement using a DC power supply E_{DC}, and (a′) its equivalent circuit. (b) By using AC power supply $e_{\mathrm{AC}}\exp(j\omega t)$ is used instead of E_{DC}. (b′) the system equivalently has two passive elements, i.e., conductance G and capacitance C.

system. The sample under the x-ray irradiation is expressed as a current source with an output equal to the photocurrent. Note that Fig. 1(a′) is a direct current (DC) circuit. In this circuit, the photocurrent is detected by a conduction current passing through conductance G built into the sample and the system. For the sake of convenience, the conduction current is denoted by "x-ray-induced conduction current $I_c(\mu)$" in this paper. The $I_c(\mu)$ is caused by the inner-shell excitation of all the atoms selected by the absorption edge energy, and has nothing to do with the valence states. Therefore, only an average x-ray absorption spectrum with no site specificity is observed in the case of a heterogeneous sample.

On the other hand, when an alternating current (AC) power supply, with angular frequency ω, $e_{\mathrm{AC}}\exp(i\omega t)$, is used as shown by Fig. 1(b), the sample can no longer be described by a real conductance G; another passive element, i.e., susceptance B proportional to the time derivation of the $e_{\mathrm{AC}}\exp(i\omega t)$, has to be taken into account. Susceptance B changes the phase between the voltage and the current, and is typified by capacitance C. The total current i_t in this system is expressed by

$$i_t = G e_{\mathrm{AC}} + j\omega C e_{\mathrm{AC}}, \tag{1}$$

where $\exp(i\omega t)$ is ignored to discuss the relative phase shift by C. In particular, the second term is known as a displacement current. In the complex plane, since the real and the imaginary parts make an orthogonal system, the displacement current is independent of the conduction current. Hence, under x-ray irradiation, the equivalent circuit has two different current sources transmitting the conduction currents $i_c(\mu_c)$ and the displacement currents $i_d(\mu_d)$ as shown in Fig. 1(b′). By analogy to the conventional XAFS measurement using the DC circuit, μ_c and μ_d are x-ray absorption coefficients measured by the conduction currents and displacement currents, respectively. In the actual system, continuous x-ray irradiation controls the sample capacitance and hence the displacement currents $i_d(\mu_d)$ due to the ac power supply. In the equivalent circuit shown in Fig. 1, the x-ray-induced change in the capacitance is observed as a variation of the displacement current (measured by A) with changing x-ray absorption i.e., $i_d(\mu_d)$. This is what led to the new term "x-ray-induced displacement current $i_d(\mu_d)$" being added to the expression of the x-ray-induced photocurrent. Since the total ion yield and the electron yield provide the same information related to the bulk, $i_c(\mu_c)$ in AC circuit [Fig. 1(b′)] is essentially the same as $I_c(\mu)$ in Fig. 1(a′). On the other hand, since $i_d(\mu_d)$ is a localized current caused by a polarized charge, it is responsive to a localized charge at electron traps, such as defects, surfaces, and interfaces. The x-ray absorption of atoms constructing these traps may make the displacement current vary, such that $i_d(\mu_d)$ comes to indicate site-specific x-ray absorption of electron traps.

Related site-specific observation techniques have been applied to a scanning probe microscope. Scanning images surveyed using the displacement current,[23] the capacitance,[24] and the Kelvin force[25] were found to provide site-specific images of defects on the surface, the trapping charge, and the surface potential.

One of the techniques for the detection of $i_d(\mu_d)$ is the capacitance XAFS measurement proposed in previous papers.[16,20] Figure 2(a) indicates the experimental setup for the capacitance XAFS measurement used in this study. In this case, a semiconductor with a defect as the electron trap is used as the sample. The deposition of an appropriate metal electrode onto the semiconductor forms the Schottky barrier diode (SBD) in the semiconductor. The band diagram of the SBD is shown in Fig. 2(b). A difference in the work function between the metal and the semiconductor qV_d forms a depletion layer. In this depletion layer, since the electron trapping level E_{trap} exceeds the Fermi level E_f by the band bending in the semiconductor, the electron is swept out. The thickness of the depletion layer d, tunable by an applied bias voltage V_b, is given by the solution of Poisson's equation,

$$d = [2\varepsilon_r\varepsilon_0(V_d - V_b)/qN_d]^{1/2}, \tag{2}$$

where q is the elementary electric charge, $\varepsilon_r\varepsilon_0$ is equal to the dielectric constant of the semiconductor, N_d is the density of the ionized electron trap, and V_d is the diffusion potential. The depletion layer with a low conductance makes a capacitor by a sandwich structure of metal/depletion layer/conductive semiconductor. The capacitance C formed by the electrode with the area of A, is given by

$$C = \varepsilon_r\varepsilon_0 A/d = [q\varepsilon_r\varepsilon_0 A^2 N_d/2(V_d - V_b)]^{1/2}. \tag{3}$$

The equivalent circuit of this system is given in Fig. 2(c) similar to Fig. 1(b′). The actual C is experimentally derived by the phase difference between i_t and e_{AC}, ϕ. From Eq. (1) and the vector diagram shown in Fig. 2(d),

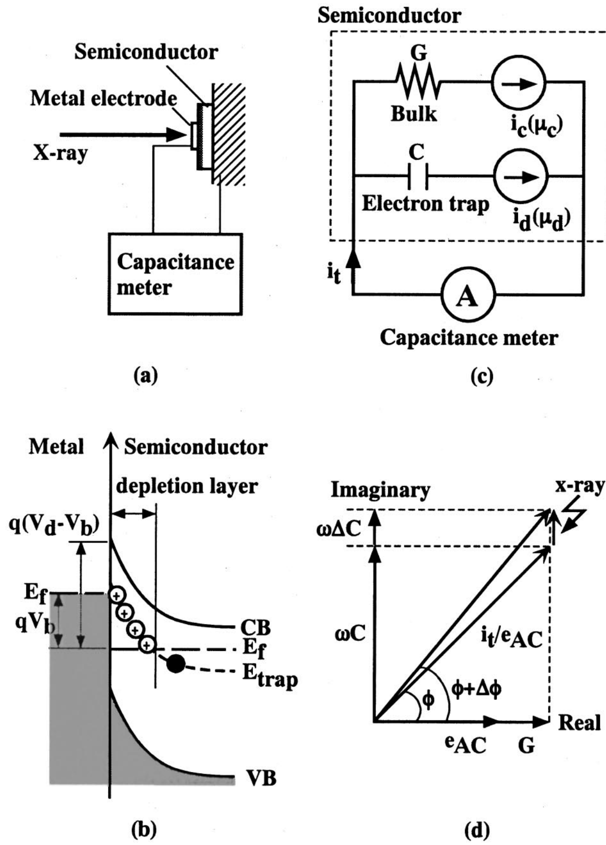

FIG. 2. (a) Experimental setup for the proposed capacitance XAFS measurement. (b) Appropriate metal deposition on the semiconductor comes to form a Schottky barrier diode, which is expressed by (c) the same equivalent circuit shown in Fig. 1(b). (d) Vector diagram showing a photocurrent expanded into a complex number.

$$\omega C = i_t \sin \phi / e_{AC}. \tag{4}$$

In an actual system, since ω and e_{AC} are given by the voltage source in the capacitance meter, the displacement current is determined by $i_t \sin \phi$.

Under x-ray irradiation, Eq. (4) is rewritten as

$$\omega(C+\Delta C) = i_t \sin(\phi+\Delta\phi)/e_{AC}, \tag{5}$$

where ΔC and $\Delta\phi$ are the additional capacitance and phase changes by the x-ray irradiation, respectively. According to $i_d(\mu_d) = i_t \sin(\phi+\Delta\phi)$,

$$\omega(C+\Delta C) = i_d(\mu_d)/e_{AC}. \tag{6}$$

Therefore, μ_d can be evaluated by the x-ray photon energy dependence of ΔC.

III. EXPERIMENTAL DETAILS

As the sample with an electron trap for the capacitance XAFS, Se-doped $Al_{0.33}Ga_{0.67}As$ (AlGaAs:Se) grown by molecular beam epitaxy was used. The substrate was (100)-oriented *n*-type GaAs. The Se was doped into the AlGaAs to a concentration of $5\times10^{17}/cm^3$ using a Knudsen cell during the growth. It is well known that a deep level of the electron trap, the *DX* center, [26,27] is formed in Se-doped $Al_xGa_{1-x}As$ ($x\sim0.3$) due to the intrinsic property of the donor impurity in zinc-blende semiconductors; chemical instability of the donor at the crystal lattice site induces a lattice distortion, resulting in the trap level instead of the donor level. Hence the deep level is uniformly distributed in the AlGaAs:Se thin film, and the number of the DX center is approximately equal to that of the donor impurity. The electron is localized within the Debye shielding length from the defect. The electric properties of the sample used in this study are described in another paper.[28] The SR experiments were performed at the SPring-8 beamline, BL10XU High Brilliance XAFS experimental station,[29,30] in Hyogo Prefecture, Japan. A Si(111) double crystal was used to monochromatize the SR beam from an in-vacuum-type undulator.[31] A rhodium-coated double mirror was used for the elimination of undesirable higher-order radiation such as third harmonics.[32] The Schottky diode was fabricated by the evaporation of an Al dot of $\sim$500 μm diameter and $\sim$100 nm thickness. The capacitance of the Schottky diode was measured by a capacitance meter, DA-1500 (Horiba Ltd.) with $\omega/2\pi=1$ MHz for AC power supply, or an impedance analyzer, 590 (Keithley) with $\omega/2\pi=100$ kHz. The typical e_{AC} was 15 mV. The substrate temperature was controlled by a closed cycle He cryostat with a 5-W heater.

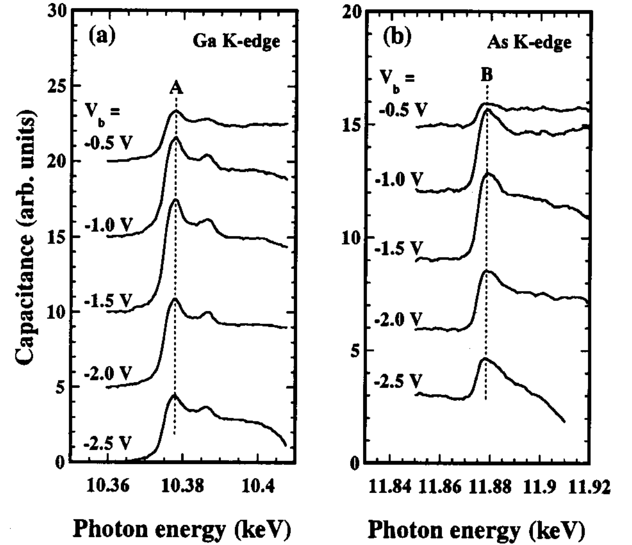

FIG. 3. X-ray photon energy dependence of the capacitance at near (a) the Ga *K* edge (10.375 keV) and (b) the As *K* edge (11.875 keV). V_b was varied from -0.5 to -2.5 V.

IV. EXPERIMENTAL RESULTS

A. Applied bias dependence

Figure 3 shows capacitance changes as a function of the x-ray photon energy at near (a) the Ga *K* edge (10.375 keV) and (b) the As *K* edge (11.875 keV). The V_b applied to the sample was varied from -0.5 to -2.5 V. The substrate temperature was fixed at 100 K. In this figure, XAFS with an edge jump and following oscillation can be observed at both absorption edges of Ga and As, indicating that the x-ray-

induced displacement current provides the XAFS spectra. The edge jump of μ_d at both absorption edges [Figs. 3(a) and 3(b)] first increases as V_b becomes negative, reaches a peak near -1.5 V, and then decreases for larger values of the back bias ($V_b < -1.5$ V). As shown in this figure, a distorted spectrum can be observed at a reduced V_b.

In the case of the conventional XAS using $I_c(\mu)$ described in Fig. 1(a), since the efficient collection of the photoelectron improves the signal to noise (S/N) ratio, a higher applied voltage is generally favorable. It is natural for a higher voltage to attain a larger current in the DC circuit, resulting in a linear dependence of $I_c(\mu)$ vs V_b. The nonlinearity of μ_d observed in Fig. 3 is an intrinsic property of AC circuits.

For a more quantitative discussion of such a nonlinearity, V_b dependences of ΔC correspondent to the x-ray absorption in the capacitance XAFS measurement are summarized in Fig. 4(a) for the Ga K edge and (b) for the As K edge (open circles). The ΔC values in (a) and (b) are represented by the resonant peak heights at the absorption edges indicated by A and B in Fig. 3, respectively. For each, the background is estimated by extrapolation from a preabsorption edge and is subtracted from the absorption peak height. A regression analysis of ΔC using a spline function showed that the maximum ΔC is obtained at ~ -1.2 V. For the analytical technique, the V_b with the maximum ΔC is favorable to secure a high S/N ratio in the XAFS measurement. This V_b with the maximum peak height is independent of the inner-shell absorption edges as indicated in Figs. 4(a) and (b), which suggests that the nonlinearity is caused by a valence property related to the defect. It is remarkable that the valence and inner-shell properties are simultaneously observable in one spectrum.

In addition, the integrations of ΔC at both K absorption edges of Ga and As are indicated by the closed circles in Fig. 4. The dashed line is the integration of the spline function in the above regression analysis of ΔC shown by the solid lines. The physical meaning of this integration will be discussed later. The integrations have gentle variations that correspond to the observed decreases of ΔC at both ends of V_b.

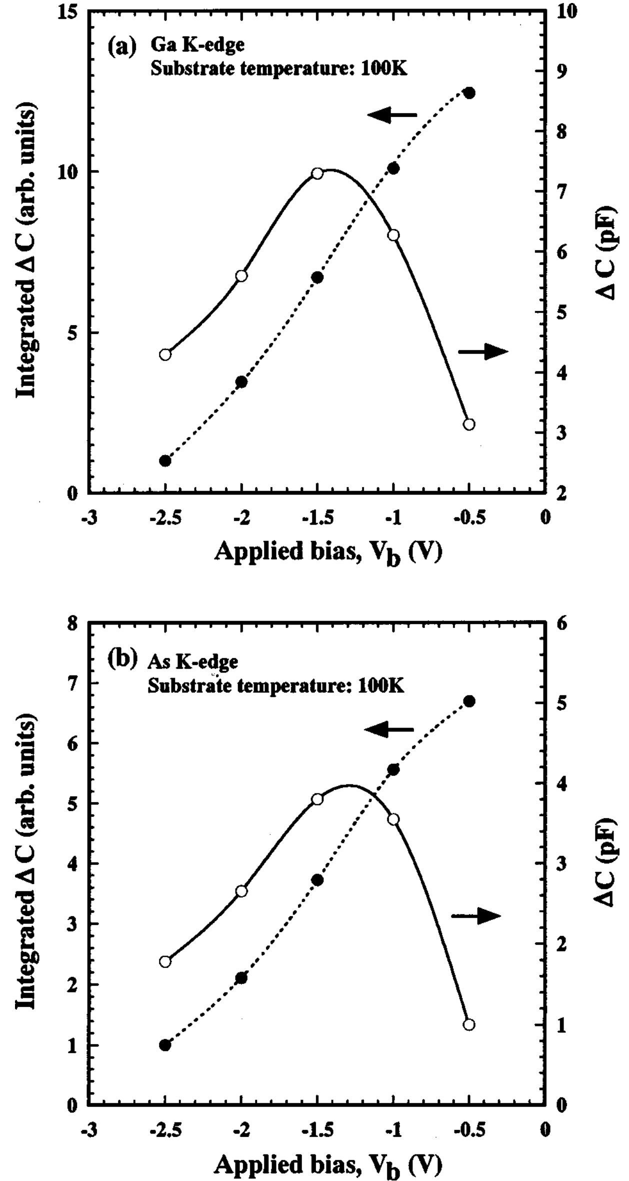

FIG. 4. V_b dependences of ΔC in capacitance XAFS spectra at (a) the Ga K edge and (b) the As K edge (open circles). The solid lines show regression analysis results of ΔC using a spline function. The integrations of ΔC at both K absorption edges of Ga and As are shown by the closed circles. The dashed line is the integration of the spline function illustrated by the solid line.

B. Substrate temperature dependence

Figure 5(a) shows the sample temperature dependence of a capacitance XAFS spectrum at the Ga K edge. The temperature was varied from 60 to 300 K. The V_b was fixed at a nearly optimal voltage of -1.5 V. As shown in this figure, the edge jump of the spectrum decreases with increasing substrate temperature. This tendency is significantly different from that of the conventional XAFS method. Figure 5(b) illustrates the conventional fluorescence XAFS spectrum for the same temperature range as Fig. 5(a). In contrast to the obvious dependence in Fig. 5(a), similar spectra independent of the temperature can be observed in Fig. 5(b). Figure 6 shows a comparison between the sample temperature dependence of the x-ray absorption in capacitance XAFS (open circles) and that in the conventional fluorescence XAFS (solid squares). The x-ray absorption of the capacitance XAFS is represented by ΔC at the resonant absorption peak denoted by A in Fig. 5(a), and its estimation procedure is the same as that described in Fig. 4. For the conventional XAFS, the corresponding absorption peak height (A' in Fig. 5) is evaluated. The amount of x-ray absorption is normalized at 60 K in each method.

The x-ray fluorescence is emitted by electron relaxation into a core hole due to the x-ray inner-shell excitation, and its emission intensity gives an absorption property equivalent to the photocurrent. Therefore, the conventional XAFS practically provides $i_c(\mu_c)$ in the equivalent circuit of this system illustrated in the inset of Fig. 6. Since the capacitance XAFS measurement observes $i_d(\mu_d)$, the temperature-dependence difference between the capacitance and the conventional

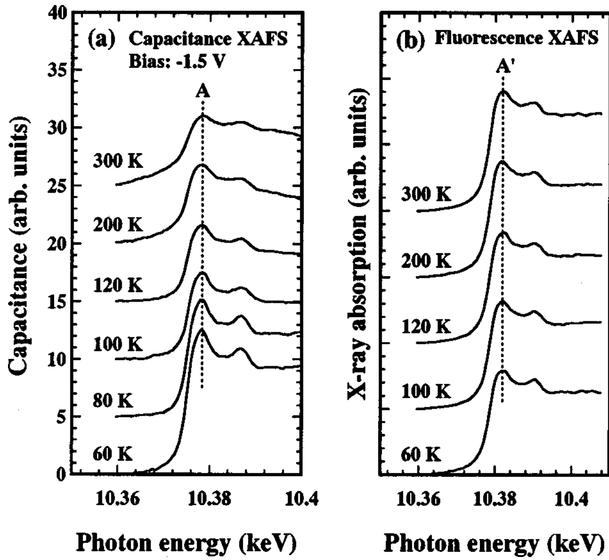

FIG. 5. (a) Sample temperature dependence of a capacitance XAFS spectrum at the Ga *K*-edge. In contrast to (a) the capacitance XAFS, similar spectra are observed in (b) the conventional fluorescence XAFS spectra in the same temperature range.

XAFS measurement shown in Figs. 5 and 6 is considered to reflect each property of μ_c and μ_d.

The μ_c given by the conventional fluorescence XAFS measures the local structure of the bulk Ga in the zinc-blende semiconductor, because the signal from a diluted electron trap in this sample is too weak to detect in a dominant signal from a perfect AlGaAs crystal structure. On the other hand, μ_d observed by the capacitance XAFS is expected to selectively provide local structure of defect in AlGaAs:Se owing to localized charge at defect. Structural analyses based on comparisons between μ_c and μ_d have been discussed in previous papers,[16,33] therefore, this paper focuses on the site specificity of x-ray-induced displacement currents. Since $i_c(\mu_c)$ results from the inner-shell excitation and the following relaxation in the energy range of ~10 keV, the temperature dependence correspondent to the energy change of ~meV is negligible, resulting in the temperature insensitive μ_c shown in Fig. 6. On the other hand, in the case of $i_d(\mu_d)$, the inner-shell absorption is observed by the variation of the polarized charge in the valence state. The comparable energy order of the substrate temperature and the valence state of ~meV, gives rise to the temperature sensitive μ_d. The reduction of μ_d at 300 K in the experimental result is considered to indicate the instability of the valence state variation by the x-ray irradiation. The thermal energy fluctuates the valence state, with the result being the reduction of information related to the inner-shell absorption via phonons.

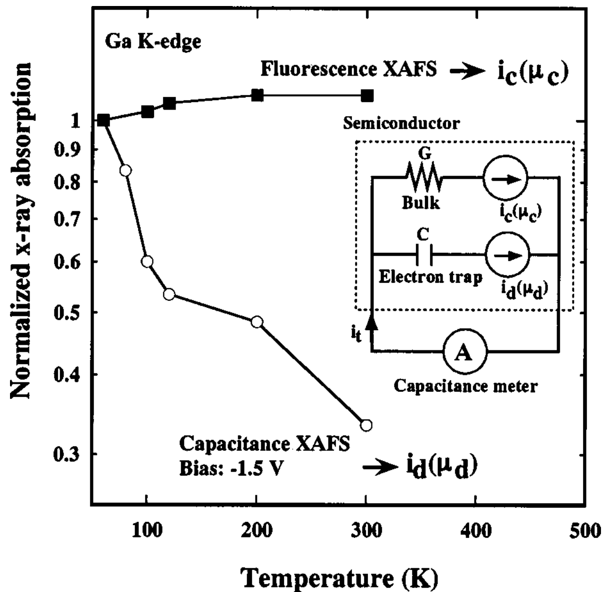

FIG. 6. Comparison between the sample temperature dependence of the x-ray absorption in capacitance XAFS (open circles) and that in the conventional fluorescence XAFS (solid squares).

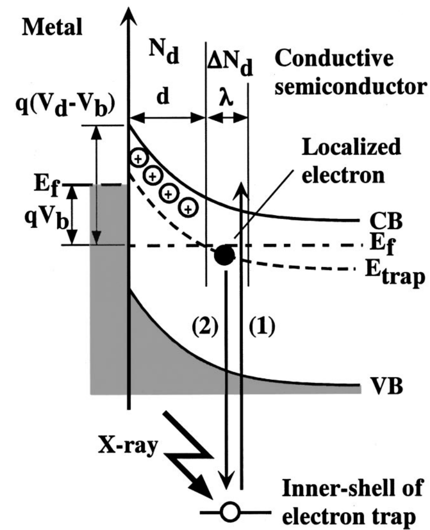

FIG. 7. Possible microscopic mechanism of the capacitance XAFS method. The x-ray absorption at a trap center and the following relaxation are equal to a delocalization of an electron from the trap center.

V. DISCUSSIONS

In the experimental results, we emphasized the inherent properties of $i_d(\mu_d)$ different from $i_c(\mu_c)$ in an electromagnetically equivalent circuit. In this section, a microscopic mechanism of the capacitance XAFS method and its interrelationship with the macroscopic properties observed in $i_d(\mu_d)$ are discussed.

Figure 7 shows the band diagram of SBD under x-ray irradiation for a possible microscopic explanation of ΔC inducement. Before the x-ray irradiation, the electron in the trap center occupies the deep level E_{trap} in the band gap of the semiconductor. When the x ray is absorbed at the trap center, a core hole is formed as illustrated in Fig. 7. The core hole should be immediately occupied by another electron typically within ~fs due to its instability. A localized electron with a weak bond energy of ~100 meV is expected to easily relax into the core hole. This sequential electron transition is identical to a delocalization of the electron from the

trap center, and increases the number of positively charged trap centers. The x-ray attenuation length of AlGaAs:Se is $>10\ \mu$m in the photon energy range for the capacitance XAFS measurements, and is sufficiently longer than the thickness of the depletion layer ($\sim$100 nm). However, since the depletion layer has no localized electron ($E_f < E_{\rm trap}$), this photoionization is induced in the restricted region deeper than d. Moreover, the positively charged trap center is immediately occupied by an electron in the conductive semiconductor ($E_f > E_{\rm trap}$). Hence, effective delocalization is induced at the edge of the depletion layer ($E_f \sim E_{\rm trap}$) as denoted by λ in Fig. 7. The localized electrons terminate the electric field in the depletion layer, so that the photoionization at λ results in a C increase. This situation is expressed by modification of N_d distribution at λ, which is approximately formalized by a modification of Eq. (3),

$$C+\Delta C=[q\varepsilon_r\varepsilon_0 A^2(N_d+\Delta N_d)/2(V_d-V_b)]^{1/2}, \qquad (7)$$

where ΔN_d denotes additionally ionized trap centers by the x-ray irradiation. By substitution of Eq. (7) into Eq. (6),

$$\omega[q\varepsilon_r\varepsilon_0 A^2(N_d+\Delta N_d)/2(V_d-V_b)]^{1/2}=i_d(\mu_d)/e_{\rm AC}, \qquad (8)$$

indicating that $i_d(\mu_d)$ is produced by ΔN_d.

Based on this microscopic model, the bias dependence of ΔC shown in Fig. 4 is formalized as follows. In our case, since ΔC is ~pF, ΔN_d is sufficiently smaller than N_d; $\Delta N_d/N_d \ll 1$. By neglecting the terms above the second order of $\Delta N_d/N_d$, Eq. (7) is approximately rewritten as

$$\begin{aligned}C+\Delta C&=[q\varepsilon_r\varepsilon_0 A^2 N_d/2(V_d-V_b)]^{1/2}(1+\Delta N_d/N_d)^{1/2}\\ &\sim[q\varepsilon_r\varepsilon_0 A^2 N_d/2(V_d-V_b)\{1+(-\Delta N_d/N_d)\}]^{1/2}\\ &=[q\varepsilon_r\varepsilon_0 A^2 N_d/2\{(V_d-V_b)+\Delta V\}]^{1/2}, \qquad (9)\end{aligned}$$

where ΔV is defined as the perturbation potential $(V_d-V_b)(-\Delta N_d/N_d)$. This equation indicates that ΔN_d by the x-ray absorption signal oscillation is equivalently represented by a small bias *change* ΔV.

The capacitance variation of SBD vs V_b (C-V characteristics) under x-ray irradiation is shown by the open circles in Fig. 8. As shown in this figure, since the conduction band becomes less than E_f at $V_b > V_d$ (charge accumulation mode), Eq. (3) cannot strictly describe the C-V characteristics at the low V_b values, resulting in a capacitance saturation distinct from $C \propto (V_d\text{-}V_b)^{-1/2}$.[34] However, the above discussion for Eq. (9) is generally applicable; ΔC at an arbitrary bias voltage can be described by assuming a small bias *change* of ΔV at V_b in Fig. 8. Typical examples are shown in Fig. 8. At $V_b \sim -1.2$ V, ΔV provides a sufficient ΔC owing to a sharp $\Delta C/\Delta V$. Since $\Delta C/\Delta V$ falls with decreasing V_b, ΔC at $V_b \sim -2.4$ V, is smaller than that at $V_b \sim -1.2$ V. At $V_b \sim -0.2$ V the charge accumulation mode also decreases $\Delta C/\Delta V$, resulting that an amplitude reduction of ΔC and wave form distortion can be observed. Consequently, ΔC at an arbitrary bias V_b is estimated by the limit of $\Delta C/\Delta V$ under $\Delta V \to 0$ at V_b, $\lim_{\Delta V\to 0}(\Delta C/\Delta V)_{Vb} = (dC/dV)_{Vb}$, and the optimal V_b for XAFS measurement is obtained at the bias voltage with the maximum $(dC/dV)_{Vb}$.

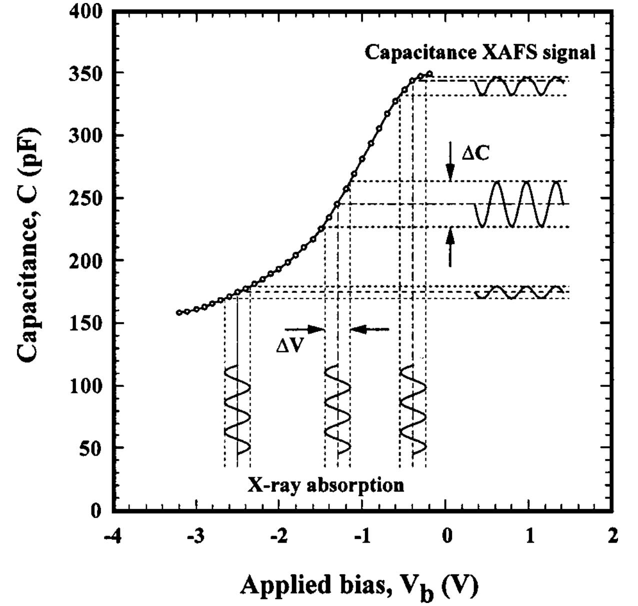

FIG. 8. C-V characteristics of SBD under x-ray irradiation (open circles) and explanation of V_b dependence of ΔC based on Eq. (9).

The open circles in Fig. 9 shows a numerically derived $(dC/dV)_{Vb}$ from the experimental result in Fig. 8. The dashed line in this figure illustrates the original C-V characteristics. The $(dC/dV)_{Vb}$ has its maximum at $V_b \sim -1.2$ V, and then it rapidly decreases above this V_b. On the other hand, below the optimal V_b, $(dC/dV)_{Vb}$ gently decreases. This tendency of $(dC/dV)_{Vb}$ reproduces the experimental result of ΔC shown in Fig. 4. The dashed line in Fig. 9 also has a similar property to the closed circles in Fig. 4, indicat-

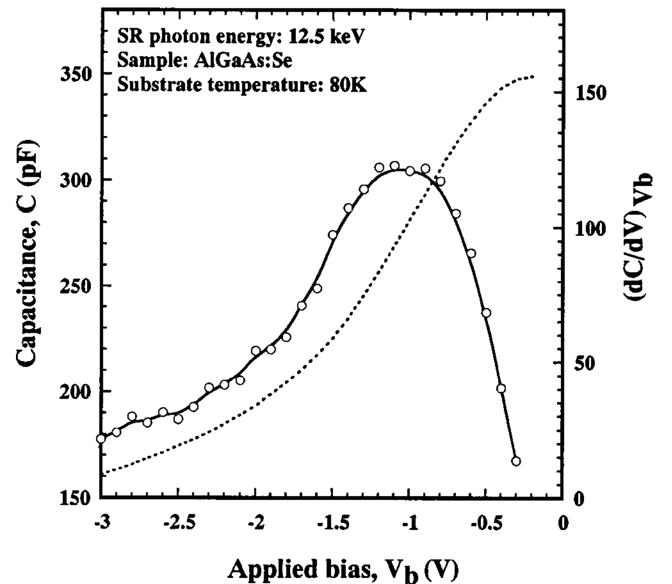

FIG. 9. Numerically derived $(dC/dV)_{Vb}$ from the C-V characteristics in Fig. 8. The dashed line illustrates the original C-V characteristics. The $(dC/dV)_{Vb}$ has its maximum at $V_b \sim 1.2$ V.

ing that the integration of ΔC in Fig. 4 corresponds to the C-V characteristics of SBD of AlGaAs:Se. The spectrum distortion observed at $V_b \sim -0.5$ V (Fig. 3) is caused by sigmoid C-V characteristics owing to the charge accumulation mode. These findings indicate that the microscopic model shown in Fig. 7 and its electromagnetic description using the equivalent circuit are adequate.

The ordinary C-V characteristics measurement based on Eq. (2) is used for the depth distribution analysis of the carrier concentration in the semiconductors, and the Debye shielding length determines the depth resolution. Though the ΔV in Eq. 9 is finite value, the corresponence between the V_b dependence of ΔC using the regression analysis (Fig. 4) and the C-V characteristics (Fig. 9) indicate that the photoionization is localized around the Debye shielding length. For the deep electron trap, since the Debye shielding length is of the atomic order, site-specific XAS of the trap is achieved by the observation of the x-ray-induced displacement current.

According to the Eqs. (3) and (7), N_d and $(N_d + \Delta N_d)$ are proportional to C^2 and $(C+\Delta C)^2$, respectively. Hence the ΔN_d at the absorption peak A in Fig. 5(a) is given by

$$\Delta N_d \propto [(C_0 + \Delta C)^2 - C_0^2], \tag{10}$$

where C_0 is background discussed in Fig. 4, and $(C_0 + \Delta C)$ is capacitance at the absorption peak. Moreover, assuming that the photoemission is approximately described by electron excitation between two different energy levels of the photoexcited and ground states, ΔN_d is expressed as

$$\Delta N_d = \Delta N_{d0} \exp(E_{\mathrm{XAFS}}/k_B T), \tag{11}$$

where ΔN_{d0} is a proportionality constant, k_B is the Boltzmann constant, and E_{XAFS} is the activation energy of the x-ray-induced photoionization process in the capacitance XAFS. Therefore, E_{XAFS} can be evaluated by the temperature dependence of ΔN_d.[20] The open circles in Fig. 10 indicate the ΔN_d variation with respect to the inverse of the temperature $1/T$. The ΔN_d is normalized at 60 K. As shown in this figure, E_{XAFS} is estimated to be 7.33 meV by fitting a solid line to the experimental data using the least-squares method. As a comparison, the carrier concentration in AlGaAs:Se under the x-ray irradiation can be estimated from the ordinary C-V characteristics (closed circles). In this experiment, the x-ray energy irradiated into the sample is fixed at 12.8 keV, which is higher than the Ga K-edge energy, so that the trap center is ionized. As shown in this figure, at high temperatures above 100 K carrier concentration is drastically increased, indicating that thermal excitation of the localized electron from the trap center becomes dominant.[26] On the other hand, in the low-temperature region below 100 K, the carrier concentration increases with decreasing temperature. This negative correlation means suppression of thermal excitation; the temperature dependence provides an effective activation energy determined by the x-ray-induced photocarrier generation and its thermal stability E_{cv}. From the fitting of this low-temperature region below 100 K, an E_{cv} of 7.68 meV is obtained, almost equal to the activation energy for E_{XAFS}. This equivalent activation energy indicates that the

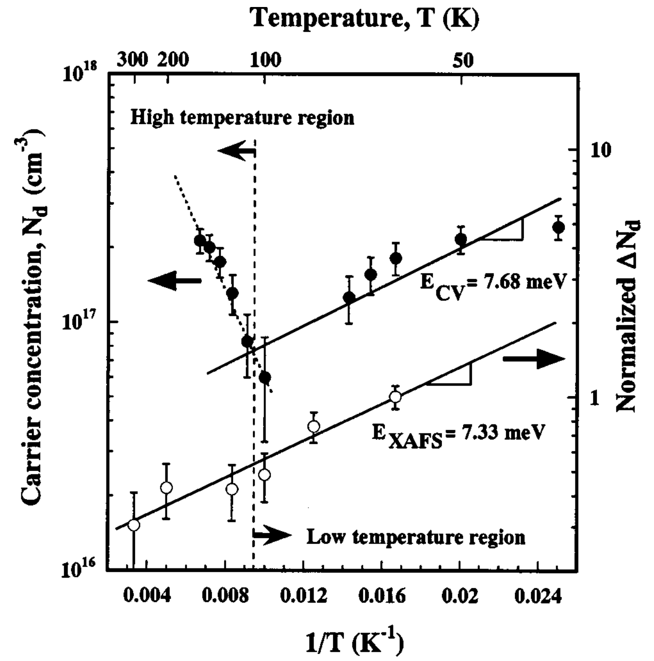

FIG. 10. Comparison between the activation process of ΔN_d in the capacitance XAFS method (open circles) and that of the carrier concentration under x-ray irradiation (closed circles).

photoemission of a localized electron in the capacitance XAFS is a generation source of x-ray-induced photocarriers in the semiconductor. The photocarriers from the defect additionally increases $i_c(\mu_c)$. The simultaneous detection of photocarriers from perfect crystals and electron trap tends to spoil the site-specificity of $i_c(\mu_c)$ observable in the conventional XAFS.

In spite of the orthogonality between $i_c(\mu_c)$ and $i_d(\mu_d)$ in complex plane, why the photocarrier is mixed from the electron trap upto $i_c(\mu_c)$ is that the inner-shell excitation process at the trap [(1) in Fig. 7] is completely the same as a perfect AlGaAs crystal site. The identical excitation processes at both sites cannot be distinguished in any way. On the other hands, note that the relaxation process difference between the trap [(2) in Fig. 7] and crystal site without E_{trap} is used for the selective observation of $i_d(\mu_d)$ in the capacitance XAFS method. Furthermore, the orthogonality between $i_c(\mu_c)$ and $i_d(\mu_d)$ operates to avoid the mixing of the photocarrier from the perfect crystal to $i_d(\mu_d)$. In fact, although clear spectra equivalent to $i_c(\mu_c)$ can be observed over the wide temperature range in the conventional XAFS measurement, $i_d(\mu_d)$ is deprived of the μ_d information at 300 K as shown in Fig. 5.

Figure 10 reveals that thermal excitation drastically increases the carrier concentration in the semiconductor at high-temperature region above 100 K, and screens the photoemission process of the localized electron. Despite the significant change in the carrier concentration, the capacitance XAFS signal keeps an E_{XAFS} of 7.33 meV in this high-temperature region. This experimental finding indicates that the electron transition process in the capacitance XAFS (Fig. 7) is independent of the conduction current. Though the conduction current in this experiment is originated from the ther-

mal excitation, this result is consistent with the independence of $i_d(\mu_d)$ from a general conduction current including $i_c(\mu_c)$, i.e., the site specificity of the capacitance XAFS.

VI. CONCLUSION

In order to achieve site-specific observation of electron traps by x-ray absorption fine structure measurement, x-ray induced displacement currents were observed via capacitance variations. In contrast to photocurrents without site specificity, displacement currents orthogonal to conduction currents are sensitive to localized charges, such that they can selectively provide structural information related to electron traps. Capacitance XAFS observations using SBD as a capacitor displayed inherent properties of these x-ray-induced displacement currents. The capacitance XAFS signal intensity was found to have a nonlinear dependence on the bias voltage applied to the sample. In addition, the electronic dynamics in a SBD under x-ray irradiation was discussed to explain the nonlinearity. Assuming additional polarized charges caused by the x-ray-induced photoionization of the trap, the macroscopic nonlinearity is formalized by this microscopic dynamics. Moreover, the temperature dependence of the capacitance XAFS was found to experimentally indicate the orthogonality, which avoids the mixing of the photocurrent from a perfect crystal site to an x-ray induce displacement current owing to a polarized charge in a defect.

ACKNOWLEDGMENTS

This work was supported by a Grant-in-Aid for Scientific Research (No. 13650476) from the Ministry of Education, Science, Sports, and Culture. The synchrotron radiation experiments were performed at SPring-8 with the approval of JASRI (Proposal No. 1999B0168-NX). The author would like to thank Ms. Y. Yoshino and Prof. K. Takarabe of Okayama University of Science for the sample preparation.

*FAX: +81-791-58-0830. Email address: ishiim@spring8.or.jp

[1] H. Kimura, M. Watanabe, K. Izumi, T. Hibiya, D. Holland-Moritz, T. Schenk, K. R. Bauchspieß, S. Schneider, I. Egry, K. Funakoshi, and M. Hanfland, Appl. Phys. Lett. **78**, 604 (2001).

[2] T. Ruf, J. Serrano, M. Cardona, P. Pavone, M. Pabst, M. Krisch, M. D'Astuto, T. Suski, I. Grzegory, and M. Leszczynski, Phys. Rev. Lett. **86**, 906 (2001).

[3] J. A. Gupta, S. P. Watkins, E. D. Crozier, J. C. Woicik, D. A. Harrison, D. T. Jiang, I. J. Pickering, and B. A. Karlin, Phys. Rev. B **61**, 2073 (2000).

[4] F. W. Lytle, D. E. Sayers, and E. A. Stern, Phys. Rev. B **11**, 4825 (1975).

[5] B.-K. Teo and P. A. Lee, J. Am. Chem. Soc. **101**, 2815 (1979).

[6] A. G. McKale, B. W. Veal, A. P. Paulikas, S.-K. Chan, and G. S. Knapp, J. Am. Chem. Soc. **110**, 3763 (1988).

[7] M. Ishii, T. Ishikawa, T. Ueki, S. Komuro, T. Morikawa, Y. Aoyagi, and H. Oyanagi, J. Appl. Phys. **85**, 4024 (1999).

[8] E. S. Marcos, M. Gil, J. M. Martínez, A. Muñoz-Páez, and A. S. Marcos, Rev. Sci. Instrum. **65**, 2153 (1994).

[9] G. D. Sanders, K. W. Kim, and W. C. Holton, Phys. Rev. B **61**, 7526 (2000).

[10] K. Streubel, M. Hammar, F. Salomonsson, J. Bentell, S. Mogg, S. Rapp, J. Jacquet, J. Boucart, C. Stark, A. Plais, F. Gaborit, E. Derouin, N. Bouché, A. Rudra, A. V. Syrbu, V. P. Iakovlev, C.-A. Berseth, O. Dehaese, E. Kapon, H. Moussa, I. Sagnes, and R. Raj, Opt. Eng. **39**, 488 (2000).

[11] J. F. Carlin, R. P. Stanley, P. Pellandini, U. Oesterle, and M. Ilegems, Appl. Phys. Lett. **75**, 908 (1999).

[12] H. Tolentino and A. R. D. Rodrigues, Rev. Sci. Instrum. **63**, 946 (1992).

[13] J. Goulon, P. Tola, M. Lemonnier, and J. Dexpert-Ghys, Chem. Phys. **78**, 347 (1983).

[14] R. F. Pettifer and A. J. Bourdillon, J. Phys. C **20**, 329 (1987).

[15] L. Solerholm, G. K. Liu, M. R. Antonio, and F. W. Lytle, J. Chem. Phys. **109**, 6745 (1998).

[16] M. Ishii, Y. Yoshino, K. Takarabe, and O. Shimomura, Appl. Phys. Lett. **74**, 2672 (1999).

[17] Y. Izumi and Hiroyasu Nagamori, Bull. Chem. Soc. Jpn. **73**, 2017 (2000).

[18] T. K. Sham, D. T. Jiang, I. Coulthard, J. W. Lorimer, X. H. Feng, K. H. Tan, S. P. Frigo, R. A. Rosenberg, D. C. Houghton, and B. Bryskiewicz, Nature (London) **363**, 331 (1993).

[19] M. Ishii, Y. Tanaka, T. Ishikawa, S. Komuro, T. Morikawa, and Yoshinobu Aoyagi, Appl. Phys. Lett. **78**, 183 (2001).

[20] M. Ishii, Y. Yoshino, K. Takarabe, and O. Shimomura, J. Appl. Phys. **88**, 3962 (2000).

[21] I. Song, B. Rickett, P. Janavicius, J. H. Payer, and M. R. Antonio, Nucl. Instrum. Methods Phys. Res. A **360**, 634 (1995).

[22] I. Watanabe, H. Tanida, S. Kawauchi, and M. Harada, Rev. Sci. Instrum. **68**, 3307 (1997).

[23] Y. Majima, S. Miyamoto, Y. Oyama, and M. Iwamoto, Jpn. J. Appl. Phys., Part 1 **37**, 4557 (1998).

[24] R. C. Barrett and C. F. Quate, J. Appl. Phys. **70**, 2725 (1991).

[25] A. K. Henning, T. Hochwitz, and J. Slinkman, J. Appl. Phys. **77**, 1888 (1995).

[26] M. Mizuta and T. Kitano, Appl. Phys. Lett. **52**, 126 (1988).

[27] D. J. Chadi, Phys. Rev. B **46**, 6777 (1992).

[28] K. Takarabe, Y. Hirano, S. Minomura, K. Matsuda, H. Ohnishi, K. Fujita, and T. Watanabe, Phys. Status Solidi B **198**, 187 (1996).

[29] H. Oyanagi, M. Ishii, C.-H. Lee, N. L. Saini, Y. Kuwahara, A. Sato, Y. Izumi, and H. Hashimono, J. Synchrotron Radiat. **7**, 89 (2000).

[30] H. Tanida and M. Ishii, Nucl. Instrum. Methods Phys. Res. A **467–468**, 1564 (2001).

[31] H. Kitamura, Rev. Sci. Instrum. **66**, 2007 (1995).

[32] T. Uruga, H. Kimura, Y. Kohmura, M. Kuroda, H. Nagasawa, K. Ohtomo, H. Yamada, T. Ishikawa, T. Ueki, H. Iwasaki, S. Hashimoto, Y. Kashihara, and K. Okui, Rev. Sci. Instrum. **66**, 2254 (1995).

[33] M. Ishii, Y. Yoshino, K. Takarabe, and O. Shimomura, Physica B **273–274**, 774 (1999).

[34] For instance, S. M. Sze, *Semiconductor Devices Physics and Technology* (Wiley, New York, 1985).